International Journal of Heat and Mass Transfer 144 (2019) 118653

Contents lists available at ScienceDirect

International Journal of Heat and Mass Transfer

journal homepage: www.elsevier.com/locate/ijhmt

Experimental study on convective boiling flow and heat transfer in a microgap enhanced with a staggered arrangement of nucleated micro-pin-fins

Liang-Han Chien [a,b], Wun-Rong Liao [c], Mohammad Ghalambaz [d,e,*], Wei-Mon Yan [a,b,*]

[a] Department of Energy and Refrigerating Air-Conditioning Engineering, National Taipei University of Technology, Taipei 10608, Taiwan
[b] Research Center of Energy Conservation for New Generation of Residential, Commercial, and Industrial Sectors, National Taipei University of Technology, Taipei 10608, Taiwan
[c] National Synchrotron Radiation Research Center, Hsin-Chu 300, Taiwan
[d] Department for Management of Science and Technology Development, Ton Duc Thang University, Ho Chi Minh City, Vietnam
[e] Faculty of Applied Sciences, Ton Duc Thang University, Ho Chi Minh City, Vietnam

ARTICLE INFO

Article history:
Received 26 May 2019
Received in revised form 2 August 2019
Accepted 27 August 2019
Available online 3 September 2019

Keywords:
Microgap
Flow boiling
Staggered nucleate micro-pin-fin
FC-72 dielectric fluid

ABSTRACT

The boiling flow and heat transfer of FC-72 in a microgap channel are experimentally addressed. The heated surface of the microgap with a test area of 10 mm × 10 mm was enhanced using a staggered array of 613 columnar micro pin fins. Inside the micro pin-fins are nucleated with a 60 μm pore and opening of 45 μm. The test surface of the channel is a square of 10 mm, and the height of the channel is 100 μm. The saturation working temperatures of FC-72 is 50 °C, the surface heat flux was up to 60 kW/m^2, and the mass flux was selected in the range of 94–275 kg/m^2 s. The on nucleated boiling temperatures (ONB), convective heat transfer coefficient, outlet dryness, and pressure drop are measured and reported. The boiling behavior of FC-72 is also recorded using an image capturing device and reported. A comparison between the superheat temperature of nucleated pin fins and plane pin fins (with no nucleation) shows that nucleation of pin fins reduces the superheat temperature. The outcomes reveal that for a high mass flux, 196–275 kg/m^2 s, the superheat temperature is high, and the degree of superheat increases as the surface heat flux increases. When the surface heat flux is high (q'' > 30 kW/m^2), the convective heat transfer is almost independent of mass flux. At the initiation flow boiling, a notable jump in the pressure drops can be seen. After that, the pressure drop increases gradually by the increase in surface heat flux. The boiling images reveal that the boiling flow initiated inside the nucleation pores of micro pin-fins.

1. Introduction

Recent developments in electronic technologies and semiconductor have increased the heat generation and power density of particularly microprocessors and high-performance chips. Despite remarkable advancement that has been made during the past decades, the thermal management of electronics devices or microprocessors is still a challenge. The non-uniform power dissipation due to the growing integration of devices in lower package sizes is another cooling issue. The heat flux at a peak chip can be several times higher than that of the adjacent regions [1]. Heat removal and the uniformity of temperature distribution at a high heat flux surface are two technological challenges [1]. A significant temperature difference among a chip can damage the mechanical and material structure of the chip and result in chip failure. Stability of the cooling system is also another essential issue. Overheating of an electrical component results in an increase of waste heat. The increase in waste heat gradually raises the temperature of the component.

Most of the available cooling systems which are based on single phase flow heat transfer are not capable of adequate cooling of high power density modules (high-performance chips) due to their low performance of heat removal from the chip surface. The latent heat of evaporation can absorb a tremendous amount of heat from a surface at adequately constant temperature difference. The phase change heat transfer has the advantage of extensive heat removal. Possible improvement in heat transfer over single-phase flow at the same mass flux due to the latent heat of vaporization makes it a promising thermal management method for high power

* Corresponding authors at: Ton Duc Thang University, Ho Chi Minh City, Vietnam (M. Ghalambaz). Department of Energy and Refrigerating Air-Conditioning Engineering, National Taipei University of Technology, Taipei 10608, Taiwan (W.-M. Yan).

E-mail addresses: mohammad.ghalambaz@tdtu.edu.vn (M. Ghalambaz), wmyan@ntut.edu.tw (W.-M. Yan).

https://doi.org/10.1016/j.ijheatmasstransfer.2019.118653
0017-9310/

Nomenclature

$\dot{m}$	the mass flow rate (kg/s)
A_c	microgap cross-sectional area (m^2)
A_p	projected area (m^2)
C_p	Fc-72 specific heat capacity (J/kg °C)
G	fluid mass flux (kg/m^2 s)
h_{fg}	evaporation latent enthalpy (J/kg)
I	heater current (A)
k	microgap thermal conductivity
k_f	FC-72 thermal conductivity (W/m °C)
P	pressure (Pa)
P_i	inlet pressure (kPa)
P_o	outlet pressure (kPa)
Q	heater input power (W)
Q''	test surface heat flux (W/m^2 °C)
Q_{loss}	heat loss (W)
T	temperature (°C)
T_{in}	inlet temperature (°C)
T_{sat}	saturation temperature (°C)
T_w	temperature of the test surface (°C)
V	heater voltage (V)

Greek symbol

ΔT_{ws}	Surface temperature difference (°C)
μ	dynamic viscosity (Pa × s)
ρ_f	fluid density (kg/m^3)
ρ_g	gas density (kg/m^3)

dissipation electronics. So that, cooling of high heat flux surfaces using boiling flow has been the subject of many recent works.

The literature review shows that the common coolants that have been used for boiling flow experiments are: water, FC-72, HFE-7000, R-134a, R-245fa, and R-123 [2]. Among these coolants, water has received much attention due to its high value of sensible and latent heat capacity, which facilitate absorption of a substantial amount of heat during the heat transfer process. The water is also the most environmentally friendly coolant. However, at atmospheric pressure, the saturation temperature of the water is 100 °C. Such a high cooling temperature is not suitable for the operation of complementary metal-oxide semiconductor electronic components [2]. Another disadvantage of water for phase change cooling in microchannels is its high liquid to vapor density ratio. A high liquid to vapor density ratio results in high void spaces with low vapor quality and high-pressure drop on vaporization [3].

Considering cooling of electrical components, dielectric coolants such as FC-72 and refrigerants are of interest due to their low saturation temperature. They are also chemically and electrically inert. The boiling temperature of many of the dielectric fluids is in the recommended range of 80–130 °C [4]. However, some refrigerants have the problem of high saturated pressure for electronic cooling applications, and application of some dielectric refrigerants are limited due to their impacts on global warming and damage of ozone layer [5]. The high-wetting nature and the low surface tension of these fluids have resulted in considerably higher superheat temperatures compared to water or other typical cooling fluids. Regarding the cooling aspects of heat transfer microchannels there are several excellent reviews [6–8]. One way to overcome the drawbacks of low heat transfer is enhancing the channel surface with etching obstacles on the surface.

Tibiriçá and Ribatski [9] reviewed various aspects of the flow boiling in microchannels such as flow patterns, heat transfer coefficient, and pressure drop. The outcomes indicate that the boiling heat transfer results in high heat transfer coefficients with the cost of high-pressure drop across the channel. They also indicated that the void fraction is an essential parameter in cooling performance of boiling heat transfer, but only a few experimental data are available in the literature. Kim and Mudawar [10] focused on the pressure drop of two-phase flow in mini/micro-channels. They argued that many relations are introduced for predicting the frictional pressure drop in mini/micro-channels. However, selecting a suitable model or correlation is confusing for thermal design engineers due to the limited validity of available literature. Kim and Mudawar [11] in another review addressed some of the concerns about anomalies that are prevalent in micro-channels. One of the concerns is the effect of choking and instabilities on the critical heat flux.

Han et al. [2] reviewed the flow boiling in plain and surface enhanced microgaps. Indeed, the micro-gaps can be considered as micro-channels with some obstacles in the passage. They divided the heat flow boiling heat transfer in microgaps into two categories of plain microgaps and enhanced surface microgaps with micro pin-fins. Considering plain microgaps, Sheehan and Bar-Cohen [12] and Sheehan et al. [13] studied the flow boiling of a dielectric liquid, FC-72, using infrared imaging techniques. They monitored the wall-temperature oscillations during a film evaporation process due to continuous local dry out and rewetting of the surface. They also monitored the wall temperature oscillations under the influence of the channel surface heat flux and flow regime. The subcooled flow-boiling of FC-72, a dielectric liquid, in a microgap for cooling of high power light-emitting diodes was investigated by Kim et al. [14,15]. The diodes were attached to the microgap channel to be cooled. The maximum heat flux was 200 kW/m^2. Various heights of microgap and two types of single-phase flow and two-phase flows were investigated. The results showed that the two-phase heat transfer coefficients were higher than that of single-phase flow. Moreover, as a general conclusion, the two-phase heat transfer is better in narrow microgaps.

Alam et al. [16] tested the influence of surface-roughness on boiling heat transfer in a microgap. They investigated the effect of various gap heights and surface-roughness on the flow boiling. The surface-roughness reduces the wall-superheat for initial boiling point. The rise of surface-roughness enhances the wall temperature uniformity, nucleation density, and local two-phase heat transfer coefficients. The surface-roughness did not affect the pressure drop, but it affected the pressure instability. The increase in surface-roughness increased the amplitude of pressure oscillations. Later, Alam et al. [17] utilized the same experimental setup and performed experiments with the aim of reducing the temperature gradient in the microgap. Outcomes show that a narrow gap reduces the flow oscillation and temperature gradients. These authors compared their results with the case of a microchannel and found that the heat transfer performance of a microgap can be better than a microchannel when the heat flux is high. The better performance of microgap was due to dominant confined slug-annular flow in the gap. However, a microchannel outperformed the microgap in low heat fluxes due to the early formation of slug-annular flow. The thermal performance of a microgap was also better than a microchannel when the mass flux was low. Han et al. [2] performed an excellent review of the flow boiling in microgaps.

Several studies have addressed boiling heat transfer over micro pin-fin enhanced surfaces in micro gaps. Kosar and Peles studied boiling flow and heat transfer of R-123a refrigerants for circular [18] and hydrofoil-shaped [19] types of micro pin-fins in staggered arrangement. The length and width of the microgap were 10 mm and 1.8 mm, respectively. The channel was narrow with 243 μm height. At the initial boiling point, the outcomes demonstrated high degrees of superheat and massive nucleation spots. At certain conditions, a minor growth in surface heat flux resulted in a rapid rise in flow oscillations, boiling behavior, temperature oscillations, and pressure oscillations. In the case of hydrofoil pin-fins [19], the heat transfer coefficient was an increasing function of heat flux until a certain point due to nucleate boiling. Then, the heat transfer coefficient was a decreasing function of heat flux up to CHF due to the increase of boiling vapor quality.

Krishnamurthy and Peles [20] addressed the boiling heat transfer of water in a microgap with the same cross section as [18,19] but the height of 250 μm. The microgap surface was enhanced with 50 μm radius circular pin-fins. The fins were arranged in staggered arrays with the pitch-to-diameter ratio of 1.5. The outcomes of this study indicate that the boiling heat transfer coefficient is almost independent of surface heat flux. Due to the essential heat transfer enhancement of fins over the channel/gap surface, various shapes and arrangement of these fins have been studied in the literature. David et al. [4] utilized staggered square pin-fins to enhance the heat transfer at the surface of a microgap and studied the boiling heat transfer behavior of R-134a. Ong et al. [21] enhanced the surface by using circular pin-fins with a staggered arrangement of 45 deg and 27 deg. Yang et al. [22] and Schultz et al. [23] also utilized the circular pin fins to enhance the two-phase heat transfer at the micro gap surface. These authors [21–23] investigated the phase change heat transfer of R1234ze as the working fluid. Piranha shape is proposed for the shape of a pin-fin to enhance the boiling heat transfer at the surface of a microgap [24] and a microchannel [25,26]. Parahovnik et al. [27] adopted a streamlined shape for the pin-fins, and Cui et al. [28] selected square shape for the pin-fins to enhance the surface heat transfer in a microgap. These authors [24–29] utilized HFE-7000 as the working fluid.

Zhang et al. [30] investigated various arrangements of square pin-fins for boiling heat transfer of FC-72 dielectric liquid in a microgap. They revealed that the fins pitch and configuration affect the critical heat flux and boiling heat transfer coefficients in a microgap considerably. Xu et al. [31] addressed the flow boiling of water in pin-fin microchannel microgap for three types of pin-fin arrays. The staggered/square pin-fins, in-line/circular pin-fins, and staggered/circular pin-fins are investigated in [31]. These authors also investigated the unstable boiling in the microchannel. The outcomes show that a pin-fin microchannel gap produces a wider stable range of flow boiling compared to that of a plain channel gap. They also revealed a short-period/small-amplitude mode and a long-period/large-amplitude mode for the temperature and pressure oscillations. In the staggered pin-fin microchannels only the short-period/small-amplitude oscillation was observed.

Kosar and Peles [32] experimentally explored the effect of various shapes of micro pin fins, including circular, hydrofoil based, cone shapes, and rectangular pin fins on the pressure drop and heat transfer of single-phase flow. The effect of various shapes of pin fins on the boiling heat transfer in investigated in the literature. For example, the fins with hydrofoil shape [33], circular shape [18,20,34], Piranha shape [35,36], streamlined shape [27]. The formation of cavities has been discussed in some of the pioneer works and later was utilized in the studies of Woodcock et al. [24], Yu et al. [29,36]. Recently, the heat transfer of micro pin fins has been reviewed in excellent work by Mohammadi and Kosar [37]. The nucleation of walls has been used in pioneer works of Kuo and Peles [38], who embedded nucleation pores in the walls of a microchannel and studied flow boiling of HFE-7000. Later, the Woodcock et al. [24] and Yu et al. [26,29,36,39] used a nucleated Piranha shape pin fin to enhance the flow boiling.

The literature review of available works on the two-phase flow boiling in microgaps and microchannels shows that the shape and arrangement of micro-fins and nucleation of pin fins significantly affect the flow boiling behavior of the working fluid. The contribution of the present study is the utilization of a staggered array of nucleated pin fins on the boiling flow and heat transfer in a microgap.

2. Experimental

The present study aims to measure the heat transfer and pressure drop of flow boiling in a microgap. The schematic view diagram of the forced convection boiling system is depicted in Fig. 1, and the details of the setup instruments are summarized in Table 1. The setup of the present experiment consists of a microgap test module, a hydraulic system, a cooling system, and a measurement system.

During the experiments, the subcooled FC-72 liquid enters the microgap. In the microgap, the liquid absorbs the surface heat flux of a hot element and undergoes the change phase due to boiling. Then, the FC-72 working fluid leaves the microgap in a two-phase/vapor state. After the microgap test module, there is a heat exchanger to cool down the liquid/vapor that left the microgap. In the condenser heat exchanger, the working fluid is cooled down and condensed to the subcooled liquid to be collected in a storage tank at the bottom of the condenser. The temperature of the subcooled liquid can be adjusted by this heat exchanger. The temperature of the condenser plate heat exchanger is controlled by the constant temperature water tank and adjusted with a temperature controller to control the saturation temperature of the text section. The experiment can be conducted after a stable saturation temperature in the experimental chamber within ±0.5 °C for thirty minutes.

The subcooled FC-72 liquid leaves the storage tank through a 10 μm large size filter. After the filter, there is a sight window to check the FC-72 status visually. Then, the working liquid enters a variable speed gear pump to be pressurized. The high-pressure FC-72 liquid moves through a flowmeter and then enters a 5 μm fine filter before entering the microgap test module and completing the cycle. It should be noted that the passages between the fins in microgap are narrow; hence, the tiny particles that may be released from the heat exchanger or other parts of the experimental setup can easily block these passages. Thus, filters are an essential part of this experiment.

The measurement system consists of a data logger, a flowmeter, several thermocouples, pressure sensors, and an image capturing system. The flow meter measures the liquid flow rate while the rotational speed of the gear pump adjusts the flow rate in the system. Three thermocouples are installed at the inlet section the microgap test module to measure the temperature of the inlet fluid. Two thermocouples are mounted at the inlet wall and well insulated while the remaining thermocouple was placed at the pipeline before the test module. A pressure gauge is mounted at the entrance of the test module, and another one is placed at the outlet of the test module to measure the absolute pressure of the experiment. A differential pressure gauge is placed between the inlet and outlet to measure the pressure drop between the inlet and outlet of the microgap test module, instantly. The time average of pressure and temperature fluctuations is considered as the pressure and temperature of the experiment and reported. The absolute pressure along with the thermocouple data in the entrance of the test module, can be utilized to estimate the subcooled state

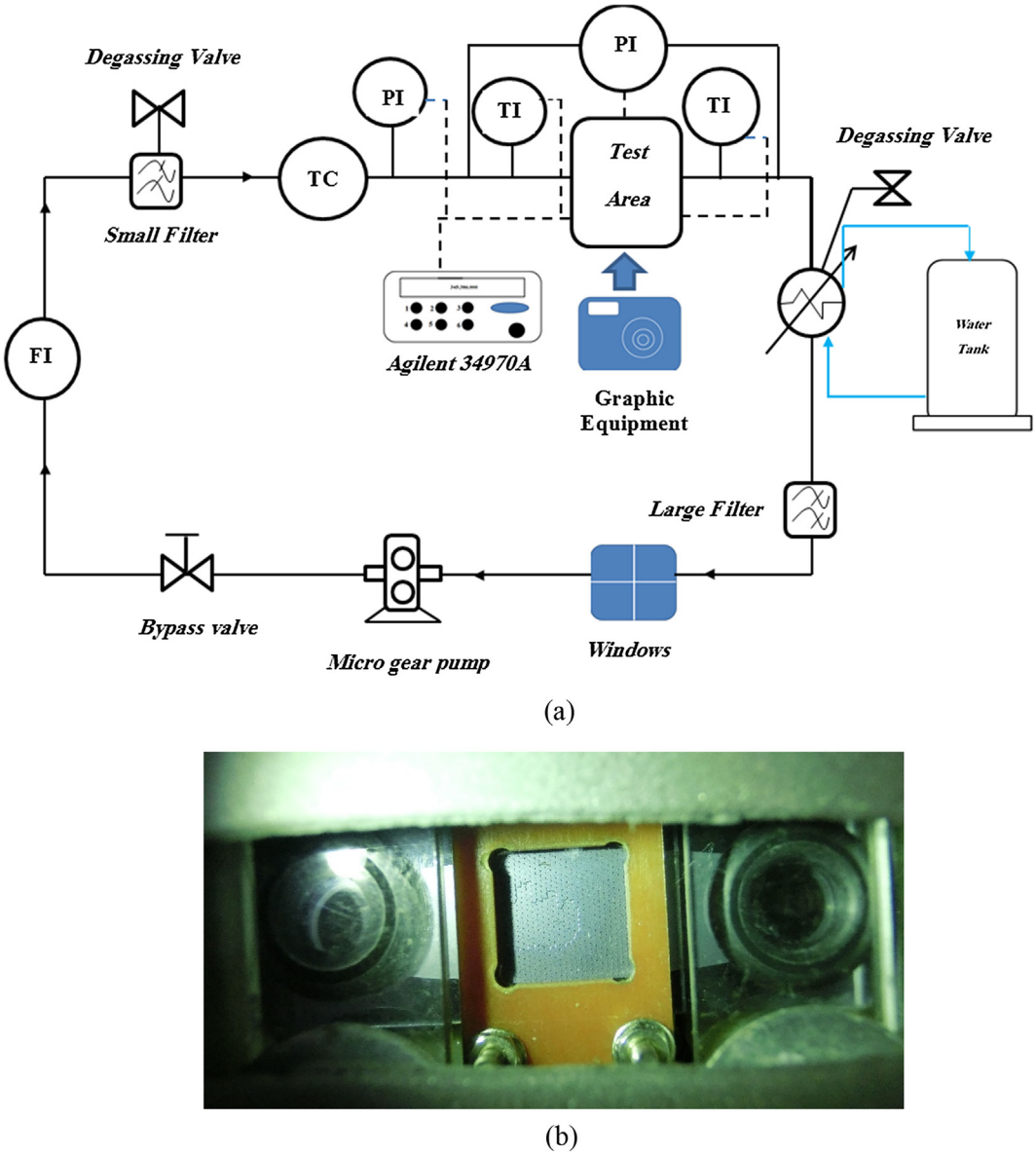

Fig. 1. (a) Schematic view diagram of the experimental setup, (b) photo of test area.

of the liquid at the inlet of the test module. Five thermocouples are utilized to measure the temperature of the microgap test surface in the microgap test module. The image capturing system consists of a digital monocular camera, a light source, and a microscope.

As mentioned, the schematic diagram of the microgap test module is illustrated in Fig. 2. The microgap test module consists of a test surface (test wafer), a heating element, a flow guiding basis, and a heat-insulating layer. As can be seen in Fig. 2, the film heater is well insulated by a 1 mm Teflon gasket layer and a 2 mm thick asbestos gasket. The insulation layers prevent the heat transfer between the stainless-steel basis and the film heater. An AC power source is utilized to provide the heating power of the thin heater. The test module was sealed using a Teflon gasket so that the FC-72 vapor cannot influence the heater and thermal insulation layers. A 2 mm thick rubber gasket is utilized for sealing of inlet and outlet of the test surface. The test surface is made of tantalum wafer of size 16 mm $\times$ 46 mm $\times$ 0.5 mm, bonded with a borosilicate glass cover of 16 mm $\times$ 46 mm $\times$ 1.1 mm by anodic bonding. The total thickness of the test module is 1.7 mm after bonding. The backside of the test surface is etched with five trenches for thermocouples. A 3 mm thick stainless steel sheet is utilized as a led to cover the top of the test surface. The led is sealed with a 2 mm rubber gasket. A window of size 10 mm $\times$ 10 mm was cut is the top cover for the test surface observation. Finally, the microgap test module was well covered with cotton to enhance the overall insulation of the test module.

The test surface is a tantalum wafer with a size of 46 $\times$ 16 $\times$ 0.5 mm (long, wide, high). An image of the final shape of the tantalum wafer is illustrated in Fig. 3(a). The microgap including the inlet, convergent and divergent passages and the columnar fins were etched on the surface with the depth of 100 μm. As mentioned, the thickness of the wafer is 500 μm, and hence, the final thickness of the test surface at the test area is 400 μm. Fig. 3(b) illustrates the back view of the test surface and the etched places for mounting the thermocouples. The drilled holes are 80 μm in diameter and 170 μm in depth. One of the thermocouples is precisely at the center of the text section. Considering a Cartesian coordinate system at the center of the test section the location of other thermocouples is as follows: (−2 mm, −2 mm), (+2 mm, −2 mm), (−3.6 mm, −3.6 mm), and (+3.6 mm, −3.6 mm).

Table 1
The list of components utilized in the experimental setup.

Type	Production (Model)	Measurement details
A light source	Luminar Ace (LA-60Me-R)	Utilized as an auxiliary device with an input voltage of 100 VAC and a 60 W metal halide lamp with an average brightness of 2,500,000 lx
AC transformer		The output power of 100 W used to power up the thin soft heater
Asbestos gasket	–	size of 16 × 20 mm^2
Data logger	Agilent's data logger (34970A)	Receives the sensors data
Digital monocular camera	Nikon (D5100)	Associated with an external magnification of 1:9 microscope and a minimum working distance of 18.5 mm
Flowmeter	AALBORG (P31A4-BAO/044-40-ST)	0–150 ml/min, the maximum error is ±1.5% of the maximum flow, i.e. ±2.25 ml/min
Liquid flow filters	–	The filters are multi-layer 5 and 10 μm grid
Micro gear-pump controller	Cole Parmer (RZ-75211-10)	Used to adjust the motor speed
Micro gear-pump head	Cole Parmer (RZ-07002-26)	The output flow rate is adjusted by changing the motor speed
Microscope	Ching Hsing Computer-Tech Ltd. (FS-230T)	The magnification range of 1 to 230 times and capability of five-segment zoom
Pressure sensor	Cole Parmer (EJA110A)	0–172.36 kPa The maximum error ±0.065% of the maximum pressure drop, i.e., ±0.112 kPa
Test wafer	Tantalum	Wafer with the test surface size of 16 × 46 × 0.5 mm^3
Thermocouples	Omega (Sheathed T-type)	Accuracy of thermocouples is ±0.5 °C
Thin film heater		10 × 10 × 0.5 mm^3
Vacuum pump	ULVAC (GVD-050A)	Maximum vacuum pressure 5 × 10^{-4} Torr
Differential pressure gauge	EW-68071-60 produced by Cole Parmer	Measure the pressure difference between the inlet and outlet of the test area. The measuring range is 0–172.369 kPa. The maximum error is ±0.25% of the maximum differential pressure, which is ±0.43 kPa

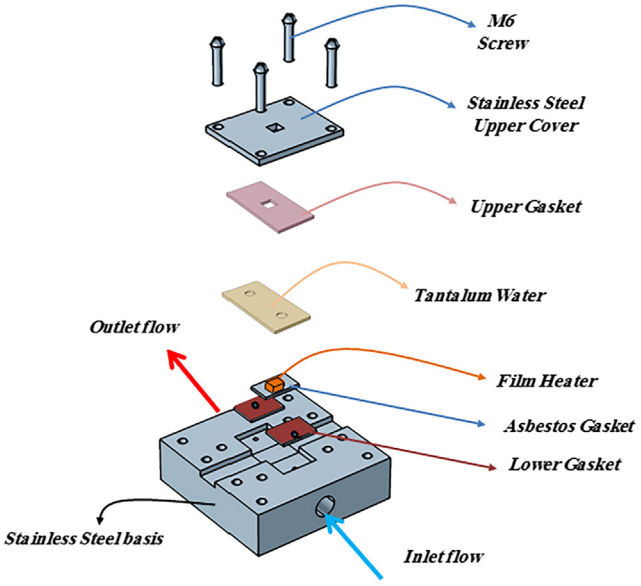

Fig. 2. The schematic view of the microgap test module.

The surface of the microgap at the test area (10 mm × 10 mm) was enhanced by etching 613 micro-columnar fins with a size of 100 μm. The cross-section of the fins is made of a 100 μm square. The center of each fin is nucleated with a 60 μm pore and opening of 45 μm. The cross-section of each fin is depicted in Fig. 4(a). As shown in Fig. 4(b), the fins are arranged in a staggered array. The fins first were etched on the wafer with no pores as depicted in Fig. 4(a) and (b), and the heat transfer were tested. Then, the pores were etched on the fins as depicted in Fig. 4(c) and (4), and the experiments were repeated.

Following [30,40–43], the working fluid is selected as FC-72 due to the stable physical and chemical properties of this dielectric fluid. Moreover, FC-72 is a non-flammable and non-toxic liquid. The boiling point of FC-72 at 1 atm is 56.6 °C. As FC-72 is a dielectric fluid, it is electrically safe for cooling of electronic components in the case of fluid leakage. The thermophysical properties of FC-72 are slightly temperature-dependent that can be evaluated using the relations introduced in [44]. Most of the electronic components are design to operate in low temperatures. Hence, the saturation temperatures of 50 °C is selected for the study of the boiling heat transfer of FC-72 in the microgap.

3. Analysis of experimental data

In order to study the effect of heat flux on the boiling flow behavior of the coolant, during each test, the mass flow rate was kept fixed, and the surface heat flux was increased. The temperatures, flow patterns, and pressure drop were monitored. The heat transfer analysis of the microgap was performed using the following relations.

Using energy balance for the test surface and heater, the generated heat in the element (Q) is equal to the total heat which reaches to the test surface plus the heat losses (Q_{loss}). Hence, the heat flux at the test surface is equal to the total heat divided by the projected test surface (A_p). The total heat of element (Q) is equal to the input current (I) times the input voltage (V). So, the test surface heat flux (q'') is evaluated as:

$$q'' = (Q - Q_{loss})/A_p = (V \times I - Q_{loss})/A_p \quad (1)$$

The heat losses from the test module, Q_{loss}, was accounted as 2–8% of the generated heat in the element. The maximum uncertainty of power supply (element heat flux) is 0.5% of output power. The heat losses were estimated by using energy balance between the amount of energy difference between the working fluid input and output of the test section. As mentioned, five thermocouples were embedded at the back of the tantalum wafer. Hence, the average temperature of the test surface (T_w) is evaluated as the average of these thermocouples. However, it should be noted that there is a thin layer of tantalum between the thermocouples and the test surface. Hence, the temperature measurements were corrected using the conduction equation by the Fourier heat conduction law as:

$$T_w = (T_{w1} + T_{w2} + T_{w3} + T_{w4} + T_{w5})/5 - q'' \times l/k \quad (2)$$

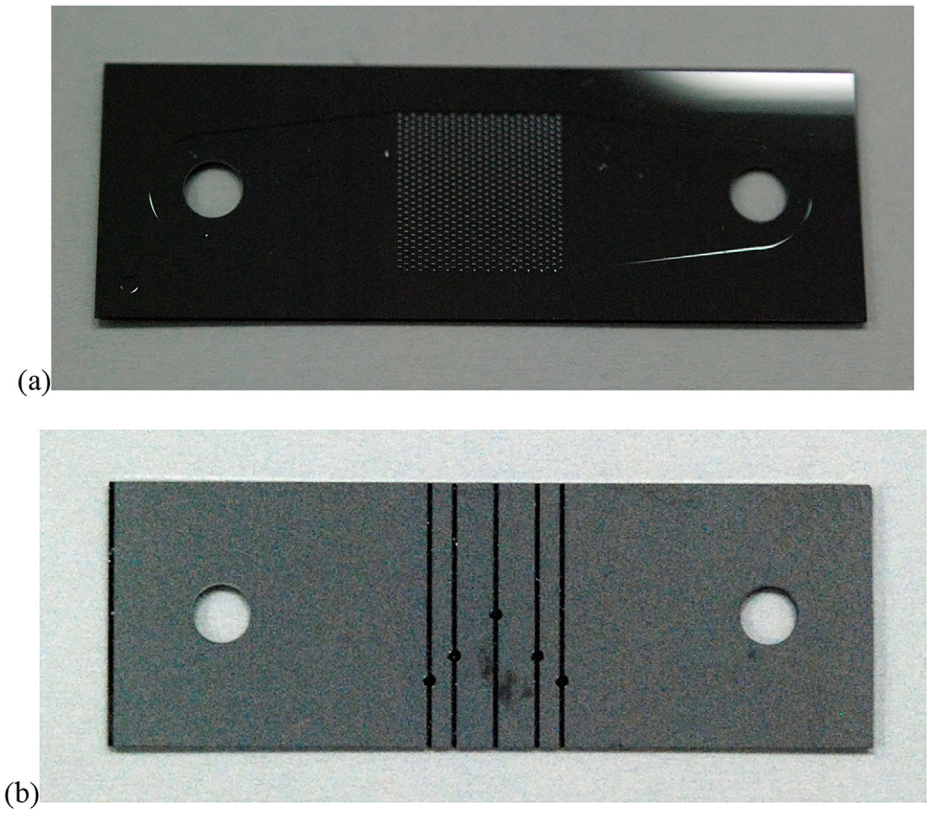

Fig. 3. The image of the wafer test surface. (a) The etched fins at front, (b) machined spaces for thermocouples at the back.

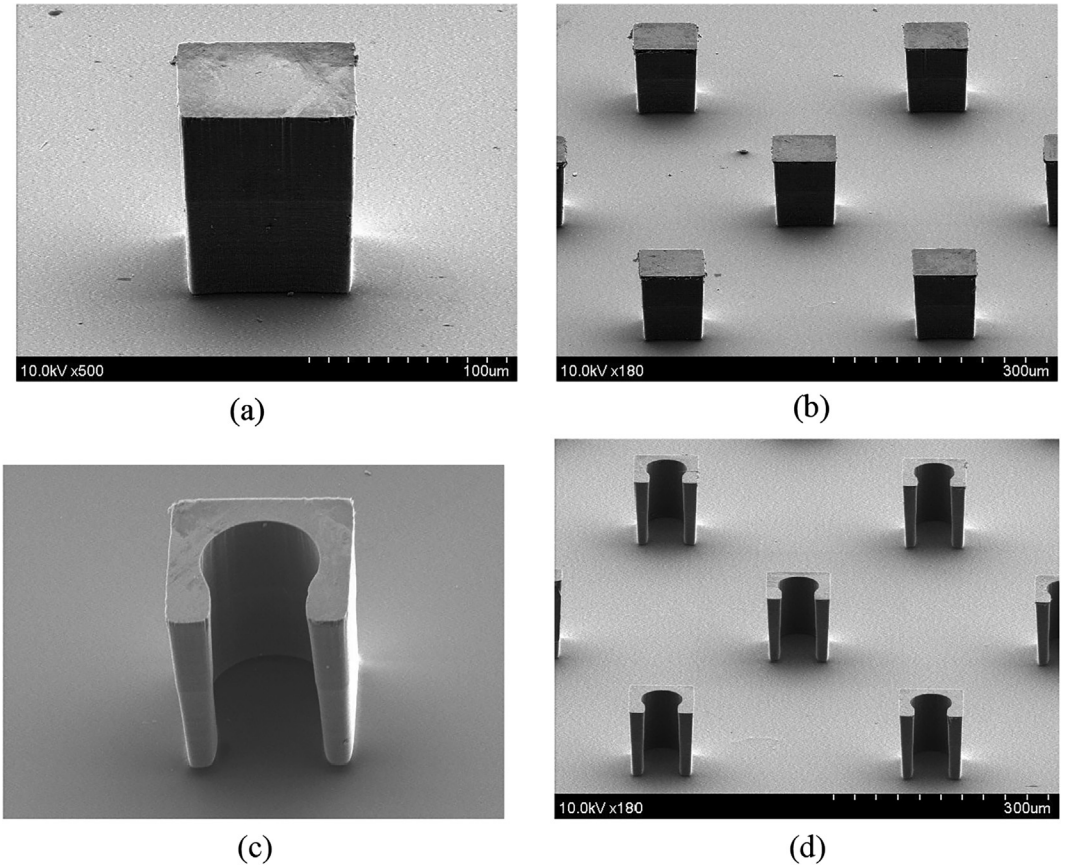

Fig. 4. The photo of etched fins. (a) The image of a single fin with no pore, the staggered array of pin fins with no pore (CNN), (c) the image of a single fin with pore size 60 μm, opening 45 μm, (d) the staggered array of pin fins with pores (C-60-45).

where l is the thickness of the wafer at the location of the thermocouple (about 230 μm), and k is the thermal conductivity of the tantalum (k = 57.6 W/mK [45]), and $T_{w1\sim5}$ are the thermocouple temperatures.

The saturation temperature (T_{sat}) is a function of saturation pressure (P_{sat}). Here, the average pressure between the inlet (P_i) pressure and outlet pressure (P_o) of the test module is adopted as the pressure inside the test module. Hence, the saturation temperature of the working fluid can be evaluated using the following relation [44] or thermodynamic tables for FC-72.

$$P_{sat}(Pa) = \exp(9.729 - -(1562/(T_{sat})) \quad (3)$$

where $P_{sat} = (P_i + P_o)/2$. Based on the calculation of T_w and T_{sat}, the surface temperature (ΔT_{ws}) is introduced as $\Delta T_{ws} = T_w - T_{sat}$. The temperature of the working fluid at the entrance of the test module (T_{in}) is evaluated as the average of the three (T_i, i = 1.0.3) mounted thermocouples as:

$$T_{in} = (T_1 + T_2 + T_3)/3 \quad (4)$$

The convection heat transfer coefficient (h) at the test surface due to boiling flow is evaluated using the surface heat flux (q'') and the temperature difference between the inlet temperature and the test surface temperature as:

$$h = q''/(T_w - T_{in}) \quad (5)$$

where q'', T_w and T_{in} were evaluated using Eqs. (1), (2) and (4), respectively. The outlet dryness was estimated using the net input heat and the mass flow rate as:

$$x_e = \frac{(Q - Q_{loss}) - \dot{m}c_p(T_{sat} - T_{in})}{\dot{m}h_{fg}} \quad (6)$$

where h_{fg} and $\dot{m}$ are the latent heat of evaporation and the mass flow rate of FC-72. The mass flowrate $\dot{m}$ can be related to the mass flux (G) of the microgap by using the microgap cross-sectional area (A_c) as:

$$G = \dot{m}/Ac \quad (7)$$

where A_c is the cross-section of the microgap with a width of 10 mm, and a height of 100 μm.

4. Results and discussion

This section aims to address the effect of working fluid temperature, mass flux, and surface heat flux on the boiling heat transfer in the microgap. The surface of the microgap was enhanced with a segregated array of nucleated columnar fins. The saturation working temperature of 50 °C is adopted for FC-72 in this experiment. The mass flux was selected in the range of 94–275 kg/m^2 s. The heating of surface commences from very low fluxes, and monastically increases until the pressure drop reaches a value higher than 15 kPa, or the surface temperature difference reaches to value higher than 100 °C. The maximum uncertainty of the results is 9%. S

Fig. 5 shows the heat transfer curves of q''-ΔT_{ws} at the mass fluxes of 94 and 196 kg/m^2 s on the surface for two cases of CNN and C-60-45. The horizontal axis is the surface superheat, and the vertical axis is the heating flux. It can be seen from the figure that in the single-phase flow heat transfer, the surface-superheat increases with the increase of the heat flux when the mass flux is fixed. The surface-superheat decreases with the increase of the mass flux. In the single-phase flow, the surface-superheat increases with nucleation of pin-fins. This is due to the low thermal conductivity of the wafer. The nucleation reduces the conductive materials of the fin, and hence, the conduction thermal resistance of the fin increases, which consequently the surface temperature raises.

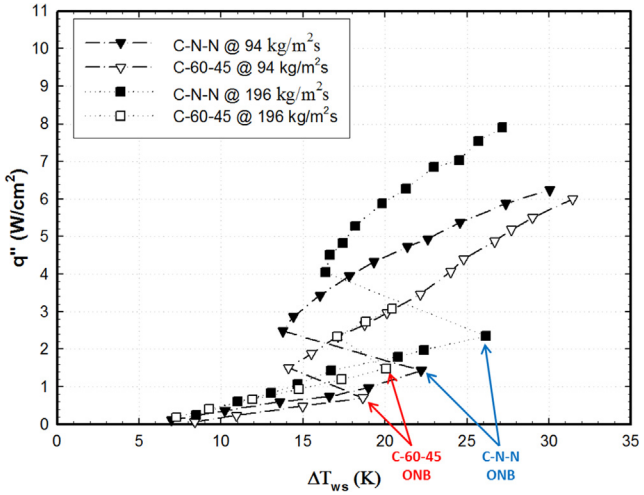

Fig. 5. The surface heat flux as a function of surface temperature difference (ΔT_{ws}) for two cases of CNN and C-60-45.

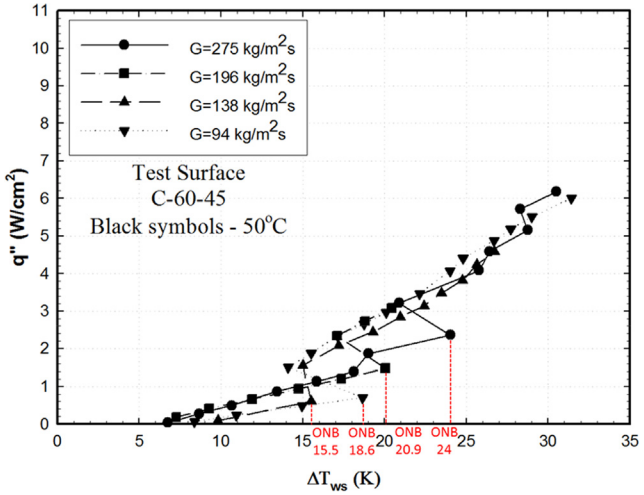

Fig. 6. The surface heat flux as a function of surface temperature difference (ΔT_{ws}) for various values of mass fluxes.

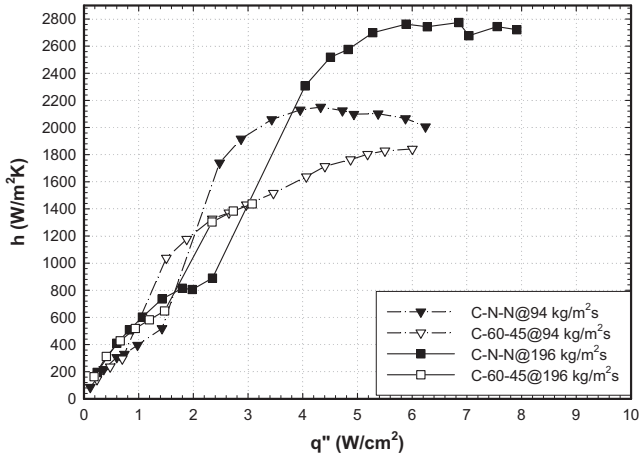

Fig. 7. The coefficient of convective heat transfer (h) as a function of surface heat flux for two mass fluxes of G = 94 kg/m^2 s and G = 196 kg/m^2 s and two cases of CNN and C-60-45.

Considering a fixed mass flux, the ONB superheat temperature of nucleated fins is much lower than that of plane fins (CNN). In the case of plane pin fins, ONB occurs at superheat temperatures of 22.2 °C and 26.1 °C for mass fluxes of 94 kg/m^2 s and 196 kg/m^2 s, respectively. In the case of nucleated pin fins, ONB occurs at supper heat temperatures of 18.6 °C and 20 °C for mass fluxes of 94 kg/m^2 s and 196 kg/m^2 s, respectively. Therefore, the nucleation of pin fins reduces the superheat ONB by 3.6 °C for the low mass flux of 96 kg/m^2 s. This reduction is 6.1 °C for the mass flux of 196 kg/m^2 s. The ONB is decreased by nucleation of pin fins presumably because the surface of the pores is easy to form a negative pressure area downstream of the fins (in the pores), which helps the bubbles to boil.

Fig. 6 illustrates the surface heat flux (q'') as a function of surface temperature difference (ΔT_{ws}) for various mass fluxes (G). As shown, at low heat flux and high mass fluxes (q = 0.7–2.36 W/cm^2 @ G = 94–275 kg/m^2 s), the heat transfer mechanism is mainly single-flow heat transfer. The surface temperature difference increases almost linearly with the increase of heat flux. As the heat flux increases, the convection boiling initiated at some superheat degrees. The surface temperature difference is a function of mass flux. The Onset of Nucleate Boiling (ONB) for various mass fluxes can be summarized as: (ΔT_{ws} = 18.6 °C, G = 94 kg/m^2 s), (ΔT_{ws} = 15.5 °C, G = 138 kg/m^2 s), (ΔT_{ws} = 20.9 °C, G = 196 kg/m^2 s), and (ΔT_{ws} = 24 °C, G = 275 kg/m^2 s). These points are marked as red in Fig. 5. At lower mass fluxes (94–138 kg/m^2 s), the required superheat is not much different. As the mass flux increases to 196–275 kg/m^2 s, the required superheat significantly increases, which results in the delay of the initial boiling. Moreover, the degree of superheat increases as the heat flux increases.

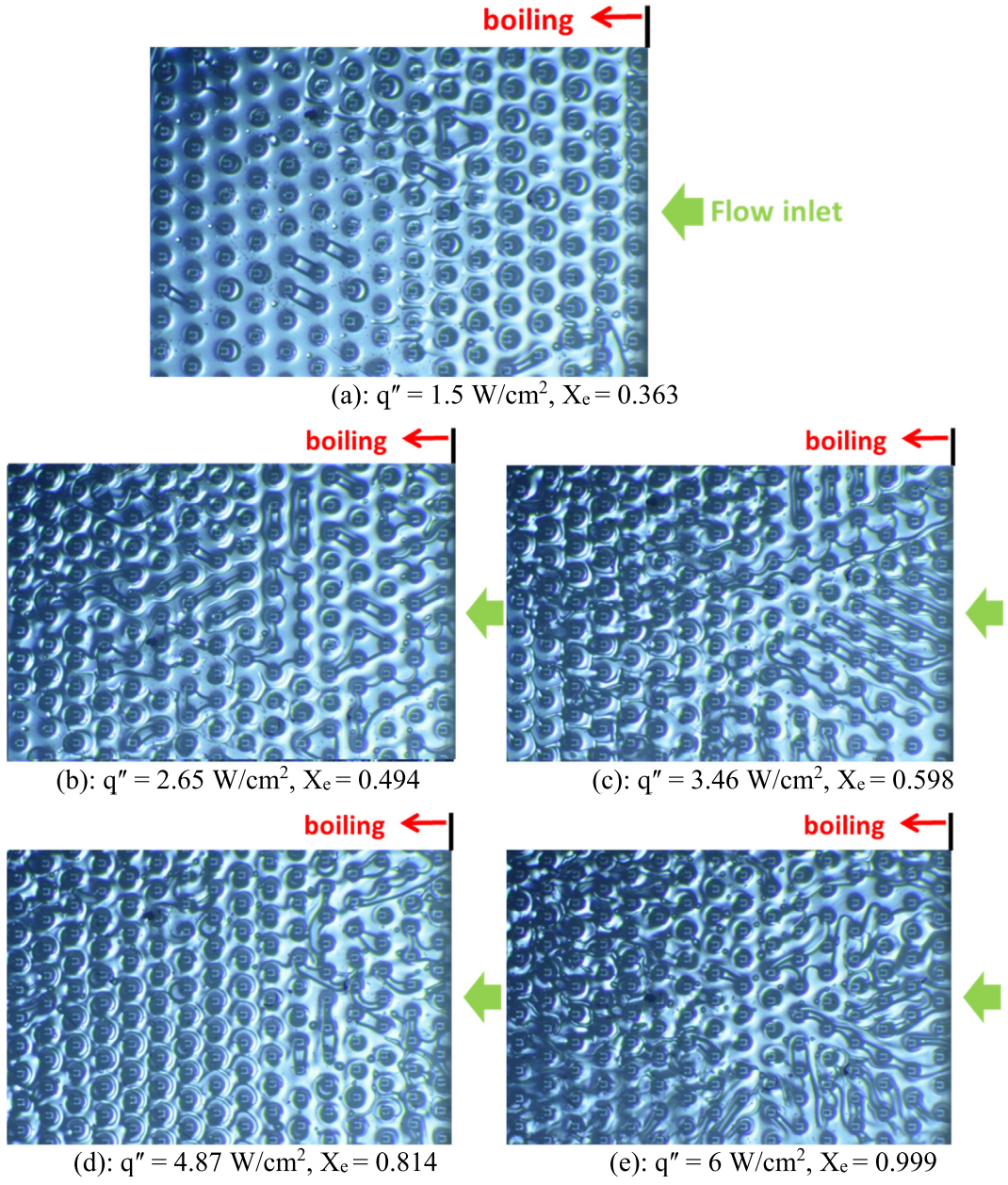

Fig. 8. Heat flux, outlet dryness and boiling flow image of the test surface when G = 94 kg/m^2 s.

Fig. 7 depicts the surface convective heat transfer coefficient (h) as a function of heat flux (q'') for two cases of CNN and C-60–45. At low heat flux, (CNN: $q'' \leqq 1.42$ W/cm^2 for mass flux of 94 kg/m^2 s, and $q'' \leqq 2.35$ W/cm^2 for mass flux of 196 kg/m^2 s), the liquid in the channel has not yet boiled, and the heat transfer mechanism is mainly a single-phase flow heat transfer. The pores of the column fins in the channel have no significant effect on the heat transfer coefficient. As seen, in the single-phase flow the heat transfer coefficient of the plain pin fins is slightly better than that of the nucleated pin fins. The presumed reason is that the nucleation pores increase the thermal resistance in the pin fin as the overall mass (overall on cross-section area) are reduced, which accordingly reduces the pin thermal efficiency. So, the heat transfer coefficient of CNN is slightly lower than that of C-60-45 single-phase flow.

As the surface heat flux increases, the fluid in the channel commence boiling, and the convection heat transfer enhances due to the contribution of the latent heat of evaporation. Fig. 7 depicts that the convection heat transfer first raises for the case of C-60-45 at a lower heat flux, and then, the heat transfer for the case of CNN rises. These significant increase in heat transfer coefficients are due to flow boiling. It is evident that the formation of bubbles in the case of nucleated pores is much easy, and hence, the flow boiling and the raise of heat transfer coefficient occurs at a lower heat flux compared to the case of CNN.

As mentioned, when the mass flux is low ($q'' \leqq 2.35$ W/cm^2), the convective heat transfer is mainly single-phase flow. Hence, the increase of the mass flux enhances the convective heat transfer. However, the onset of boiling phenome changes the regime of heat transfer. Assuming a constant amount of surface heat flux, the

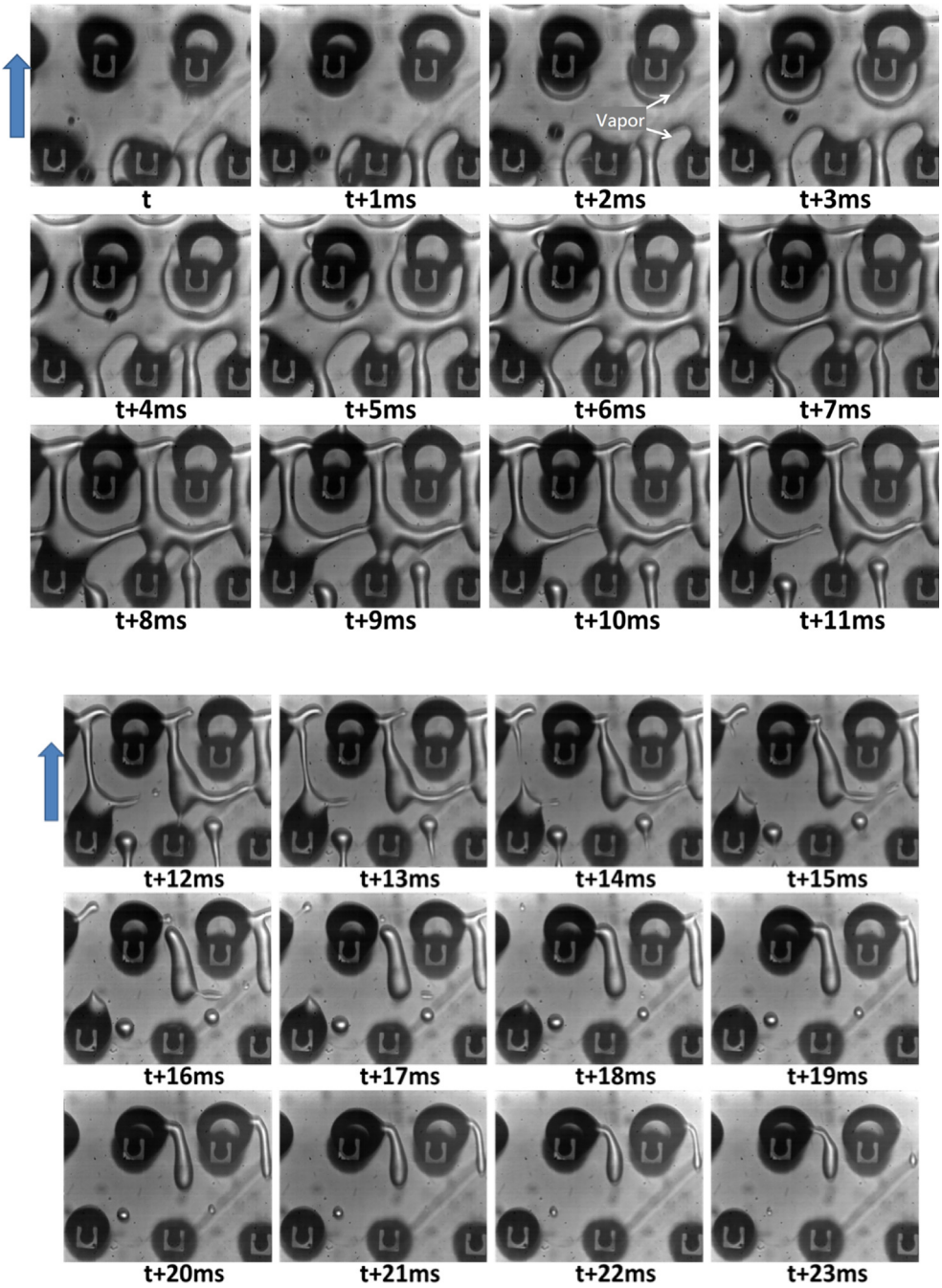

Fig. 9. The boiling flow spectrum over columnar fins when $G = 94$ kg/m^2 s and $q'' = 0.7$ W/cm^2.

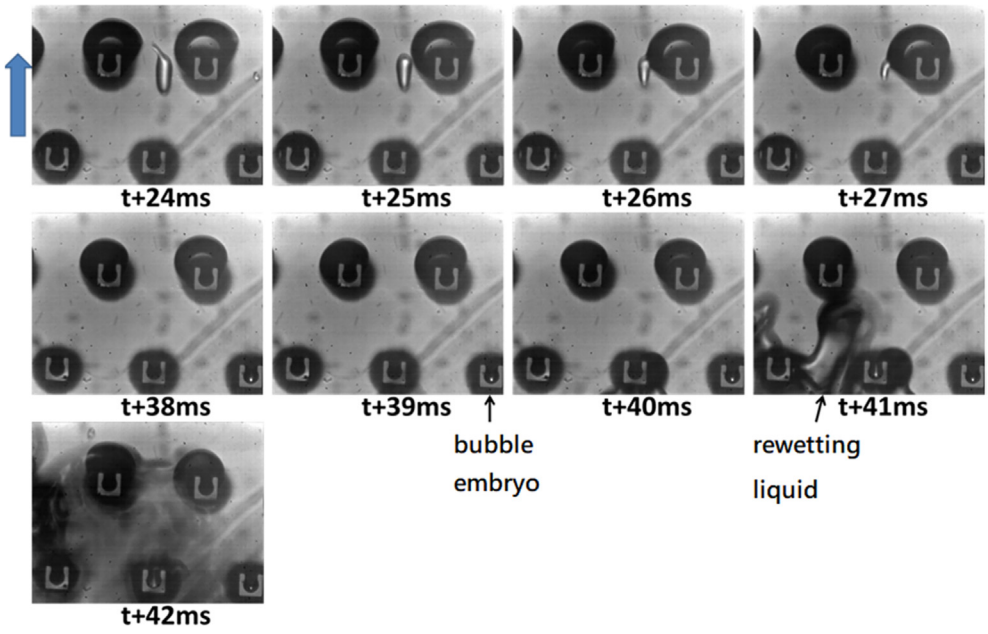

Fig. 9 (*continued*)

boiling phenome first occurs in a channel with a lower mass flux. When boiling heat transfer occurs, the heat transfer coefficient enhances dramatically. For instance, as seen in Fig. 7, the convective heat transfer coefficient of 94 kg/m^2 s is much higher than that of 196 kg/m^2 s when q'' = 2 W/cm^2.

For high heat fluxes, the convective heat transfer is almost independent of mass flux. In the case of G = 196 kg/m^2 s and $q'' \geqq 3.07$ W/cm^2, some fluctuations in measurements can be seen. In this region, the bubbles are large, the departure of these bubbles squeeze the inlet liquid causing the flow rate of the flowmeter to fluctuate notably, and the test surface produces a cyclical change of boiling and non-boiling status. At this time, the surface temperature of the wafer also fluctuates up and down.

Fig. 8 illustrates the images of boiling flow patterns for the case of G = 94 kg/m^2 s. Below each figure, the magnitude of heat flux and the outlet dryness are written. The green arrow shows the direction of flow. The boiling line indicates the commencing of the boiling. The value of heat flux can be used to link these images to the results of Figs. 6 and 7. In Fig. 8(a), it can be seen that FC-72 is in the liquid state in most of the surface area. Around the nucleated fins, there are small circular regions occupied with vapor. Attention to these circular regions shows that there are some jet shape vapor formations at the opening side of the nucleated fins. These jet shapes show the contribution of the nucleation pores on the boiling behavior of FC-72.

In the case of low heat flux, 0.67 W/cm^2, the initial boiling first occurs in the back part of the channel surface, and the boiling gas flows to the upstream direction of the channel only in a portion of the channel surface area. The vapor around the fins forms a continuous vapor area which moves toward the outlet of the channel. By the increase of the heat flux to 2.65 W/cm^2 in Fig. 8(b), some of the small regions of vapor around the columns were joined. These regions mainly are limited to cover one or two fins. By the further increase of heat flux to 3.46 W/cm^2 in Fig. 8(c), separate branches of vapor and liquid can be distinguished. In Fig. 8 (d), only a few liquid branches are left, and most of the surface area is occupied with vapor. In Fig. 8(e), only a few small points have remained in the liquid form, and almost all of the test surface is filled with vapor. The flow spectrum transformation process in Fig. 8(a)–(d) are cell flow, block flow, droplet/block flow, and droplet flow, respectively. In Fig. 8(e), that most of the liquid from all channels passes between the fins and forms a liquid, gas diversion multiple independent flow channels; hence, the flow field patterns can be represented as an annular flow spectrum.

In Fig. 8, some jet shape vapors next to the opening were observed. Here, one cycle of boiling will be studied in detail to explore the effect of the nucleated shape of fins on the boiling heat transfer. Fig. 9 shows a close view of the boiling flow spectrum (t ~ t + 42 ms) at a mass flux of 94 kg/m^2 s with a low heat flux of 0.7 W/cm^2 for an array of fins. As seen, due to the staggered arrangement of the fins, the fluid easily separated and combined to produce disturbances, and the intermittent fins act as heat transfer boosters and further charge the bubbles, and indirectly they increase the heat transfer coefficient. The blue arrow shows the fluid direction. Starting from a liquid ball (t), after continuously absorbing heat, gas is generated around the fin and gradually enlarges (t + 2 ~ 10 ms), and the liquid flows through the narrow branch between the gas. At this time, the flow field type is like a cell, known as cell flow, as the heat absorption increases, the tiny liquid branch will be disconnected by evaporation (t + 11 ~ 17 ms), and some of the remaining liquid on the channel surface will be combined with the liquid ball in the pore (t + 18 ~ 27 ms). The liquid ball will gradually shrink with the absorption of heat until the entire pore is dry. When the pores of the test surface are mostly surrounded by vapor, the upstream liquid will flow in the test surface to re-wet surface. The intermittent or continuous nucleation boiling effect (t + 38 ~ 42 ms) is generated, and the overall view of the nucleation process was shown in Fig. 7.

Fig. 10(a) and (b) depict the boiling flow patterns for a low heat flux of 0.7 W/cm^2 and high heat flux of 4.87 W/cm^2, respectively. The blue arrow indicates the direction of the flow. In the case of low heat flux (Fig. 10 (a)), a regular flow pattern of cells occurs when liquid flows into the test surface. The liquid flows regularly through the narrow branches between the vapor bubbles. In the case of high heat flux (Fig. 10(b)), the test surface temperature is high, and the liquid flowing through the narrow branch is natural to boil on the surface, exhibiting a liquid-gas mixed boiling flow field type. This is because of the staggered arrangement of fins which mix the liquid and gas branches adequately.

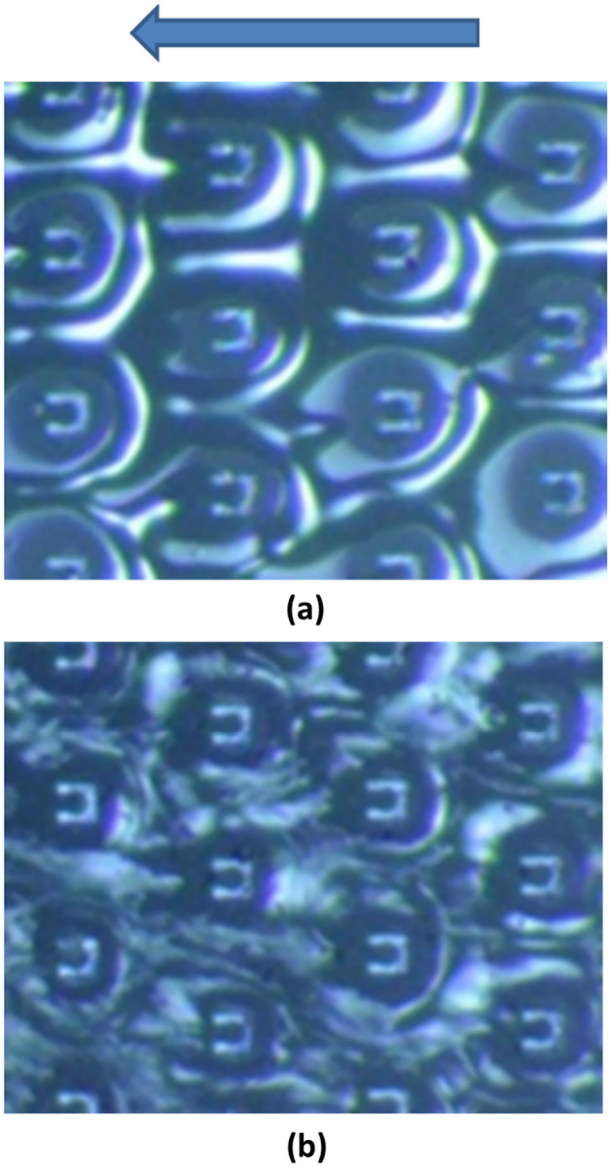

Fig. 10. Flow boiling spectrum when $G = 94\ kg/m^2\ s$. (a) cell flow field at $q'' = 0.7\ W/cm^2$, (b) liquid-gas mixed boiling flow field at $q'' = 4.87\ W/cm^2$.

5. Conclusion

An experimental test setup was built to study the boiling heat transfer in a microgap. The heated part of the test surface with the size 10 mm was enhanced with 613 micro pin-fins to improve boiling heat transfer in the microgap. The columnar fins were arranged in a staggered array. FC-72 as a dielectric fluid was adopted as the working fluid with the saturation temperature of 50 °C. The effect of surface heat flux and mass flux of the working fluid on the ONB, heat transfer coefficient, and pressure drop in microgap were addressed. The boiling flow patterns over the test surface are recorded and discussed. The key results of the present work can be summarized as follows:

1. At low heat flux and high mass fluxes, the surface temperature difference increased linearly with the increase of heat flux due to the single-phase dominant heat transfer mechanisms. At the moderate heat fluxes, in which there were some degrees of boiling, the surface temperature difference was a function of mass flux.
2. The nucleation of pin fins decreases the heat transfer coefficient at single-phase flow, but the nucleation decreases superheat temperature on boiling heat transfer and result in a better convective heat transfer coefficient at early stages of boiling heat transfer.
3. Generally, the increase of mass flux increased the degree of ONB superheats, resulting in postponing of ONB. The maximum value of ONB superheat temperature was observed as $\Delta T_{w\text{-}s} = 24\ °C$ in the case of $G = 275\ kg/m^2\ s$.
4. The convective heat transfer coefficient (h) increased with the increase of the heat flux. Transition to flow boiling induced a rapid increase in the magnitude of convective heat transfer. As mentioned, the increase in mass flux delayed ONB. Thus, the coefficient of the convective heat transfer for a low mass flux could be higher than that of a high mass flux due to a delay in ONB.
5. The pressure drop was minimal and almost constant before ONB in a single-phase flow regime with low surface heat flux. ONB induced a significant jump in the pressure drop. By the increase of the heat flux, the pressure drop across the microgap was increased gradually.
6. At ONB there are few vapor regions around the nucleated fins. Around the opening of fins a jet shape vapor regions were observed confirming the contribution nucleation pores on initial boiling point. By the increase of heat flux, the vapor regions extend and join each other. By the further increase of heat flux some distinct branches of vapor and liquid could be observed. When the heat flux is high, there are only a few liquid sites, and the test surface was mostly covered with vapor.

In the present study, a staggered fin arrangement with a fixed pore shape was studied. The images of flow boiling show that the first bubbles are formed at the opening of nucleated pores and around the fins. Hence, the arraignment of columnar pin-fins and the shape of fins can be two key parameters, controlling ONB and boiling heat transfer of FC-72 in the microgap. The flow boiling for various the arrangement of columnar fins, and various sizes of pores and their openings can be subject of future studies.

Declaration of Competing Interest

The authors declared that there is no conflict of interest.

Acknowledgements

The authors appreciate the financial support from Ministry of Science and Technology, Taiwan, under grant number MOST 101-2221-E-027-044-MY2. The authors also acknowledge the financial support by the “Research Center of Energy Conservation for New Generation of Residential, Commercial, and Industrial Sectors” from The Featured Areas Research Center Program within the framework of the Higher Education Sprout Project by the Ministry of Education (MOE) in Taiwan.

References

[1] S.S. Murshed, C.N.J.R. De Castro, S.E. Reviews, A critical review of traditional and emerging techniques and fluids for electronics cooling, Renew. Sustain. Energy Rev. 78 (2017) 821–833.
[2] X. Han, A. Fedorov, Y.J. Joshi, Flow boiling in microgaps for thermal management of high heat flux microsystems, J. Electron. Packag. 138 (4) (2016) 040801.
[3] S. Klein, Engineering Equation Solver, Academic Professional Software, 2015.
[4] T. David, D. Mendler, A. Mosyak, A. Bar-Cohen, G. Hetsroni, Thermal management of time-varying high heat flux electronic devices, J. Electron. Packag. 136 (2) (2014) 021003.
[5] W.T. Tsai, Environmental risk assessment of hydrofluoroethers (HFEs), J. Hazard. Mater. 119 (1–3) (2005) 69–78.

[6] Y.K. Prajapati, P. Bhandari, Flow boiling instabilities in microchannels and their promising solutions–a review, Exp. Therm Fluid Sci. 88 (2017) 576–593.
[7] A. Abdollahi, R.N. Sharma, A. Vatani, Fluid flow and heat transfer of liquid-liquid two phase flow in microchannels: a review, Int. Commun. Heat Mass Transf. 84 (2017) 66–74.
[8] A. Mohammadi, A.J.N. Koşar, M.T. Engineering, Review on heat and fluid flow in micro pin fin heat sinks under single-phase and two-phase flow conditions, Nanoscale Microscale Thermophys. Eng. 22 (3) (2018) 153–197.
[9] C.B. Tibiriçá, G. Ribatski, Flow boiling in micro-scale channels–Synthesized literature review, Int. J. Refrig. 36 (2) (2013) 301–324.
[10] S.M. Kim, I. Mudawar, Review of databases and predictive methods for pressure drop in adiabatic, condensing and boiling mini/micro-channel flows, Int. J. Heat Mass Transf. 77 (2014) 74–97.
[11] S.M. Kim, I. Mudawar, Review of two-phase critical flow models and investigation of the relationship between choking, premature CHF, and CHF in micro-channel heat sinks, Int. J. Heat Mass Transf. 87 (2015) 497–511.
[12] J. Sheehan, A. Bar-Cohen, Spatial and temporal wall temperature fluctuations in two-phase flow in microgap coolers, in: ASME 2010 International Mechanical Engineering Congress and Exposition, American Society of Mechanical Engineers, 2010, pp. 1701–1708.
[13] J. Sheehan, D.W. Kim, A. Bar-Cohen, Thermal imaging of two-phase coooled microgap channel wall, in: ASME 2009 InterPACK Conference Collocated with the ASME 2009 Summer Heat Transfer Conference, 2009, pp. 491–499.
[14] D.W. Kim, E. Rahim, A. Bar-Cohen, B. Han, Thermofluid characteristics of two-phase flow in micro-gap channels, in: Thermal and Thermomechanical Phenomena in Electronic Systems, 2008, ITHERM, 2008, pp. 979–992.
[15] D.W. Kim, E. Rahim, A. Bar-Cohen, B. Han, Direct submount cooling of high-power LEDs, IEEE Trans. Compon. Packag. Technol. 33 (4) (2010) 698–712.
[16] T. Alam, P.S. Lee, C.R. Yap, L. Jin, Experimental investigation of local flow boiling heat transfer and pressure drop characteristics in microgap channel, Int. J. Multiph. Flow 42 (2012) 164–174.
[17] T. Alam, P.S. Lee, C.R. Yap, L. Jin, A comparative study of flow boiling heat transfer and pressure drop characteristics in microgap and microchannel heat sink and an evaluation of microgap heat sink for hotspot mitigation, Int. J. Heat Mass Transf. 58 (2013) 335–347.
[18] A. Koşar, Y. Peles, Convective flow of refrigerant (R-123) across a bank of micro pin fins, Int. J. Heat Mass Transf. 49 (17–18) (2006) 3142–3155.
[19] A. Koşar, Y. Peles, Boiling heat transfer in a hydrofoil-based micro pin fin heat sink, J. Int. J. Heat Mass Transf. 50 (5–6) (2007) 1018–1034.
[20] S. Krishnamurthy, Y. Peles, Flow boiling of water in a circular staggered micro-pin fin heat sink, Int. J. Heat Mass Transf. 51 (5–6) (2008) 1349–1364.
[21] C.L. Ong, S. Paredes, A. Sridhar, B. Michel, T. Brunschwiler, Radial hierarchical microfluidic evaporative cooling for 3-d integrated microprocessors, in: 4th European Conference on Microfluidics, Limerick, Ireland, Dec, 2014, pp. 10–12.
[22] F. Yang, M. Schultz, P. Parida, E. Colgan, R. Polastre, B. Dang, C. Tsang, M. Gaynes, J. Knickerbocker, T. Chainer, Local measurements of flow boiling heat transfer on hot spots in 3D compatible radial microchannels, ASME 2015 International Technical Conference and Exhibition on Packaging and Integration of Electronic and Photonic Microsystems, 2015, pp. V003T010A006-V003T010A006..
[23] M. Schultz, F. Yang, E. Colgan, R. Polastre, B. Dang, C. Tsang, M. Gaynes, P. Parida, J. Knickerbocker, T. Chainer, Embedded two-phase cooling of large 3D compatible chips with radial channels, ASME 2015 International Technical Conference and Exhibition on Packaging and Integration of Electronic and Photonic Microsystems, 2015, pp. V003T010A007-V003T010A007..
[24] C. Woodcock, X. Yu, J. Plawsky, Y. Peles, Piranha Pin Fin (PPF)—Advanced flow boiling microstructures with low surface tension dielectric fluids, Int. J. Heat Mass Transf. 90 (2015) 591–604.
[25] X. Yu, C. Woodcock, Y. Wang, J. Plawsky, Y. Peles, Enhanced subcooled flow boiling heat transfer in microchannel with Piranha Pin Fin, J. Heat Transf. 139 (11) (2017) 112402.
[26] X. Yu, C. Woodcock, Y. Wang, J. Plawsky, Y. Peles, A comparative study of flow boiling in a microchannel with piranha pin fins, J. Heat Transf. 138 (11) (2016) 111502.
[27] A. Parahovnik, Y. Wang, Y. Peles, Transient local resolution of flow boiling in a microchannel with a sreamlined pin fin, 16th International Conference on Nanochannels, Microchannels, and Minichannels, American Society of Mechanical Engineers, 2018, pp. V001T002A001-V001T002A001.
[28] F. Cui, F. Hong, P. Cheng, Comparison of normal and distributed jet array impingement boiling of HFE-7000 on smooth and pin-fin surfaces, Int. J. Heat Mass Transf. 126 (2018) 1287–1298.
[29] X. Yu, C. Woodcock, Y. Wang, J. Plawsky, Y. Peles, Enhanced subcooled flow boiling heat transfer in microchannel with Piranha pin fin, J. Heat Transf. 139 (2017) 112402.
[30] Y. Zhang, J. Zhou, W. Zhou, B. Qi, J. Wei, CHF correlation of boiling in FC-72 with micro-pin-fins for electronics cooling, Appl. Therm. Eng. 138 (2018) 494–500.
[31] F. Xu, H. Wu, Z. Liu, Flow patterns during flow boiling instability in silicon-based pin-fin microchannels, J. Heat Transf. 140 (3) (2018) 031501.
[32] A. Kosar, Y. Peles, TCPT-2006-096. R2: micro scale pin fin heat sinks—parametric performance evaluation study, IEEE Trans. Compon. Packag. Technol. 30 (4) (2007) 855–865.
[33] A. Kosar, B. Schneider, Y. Peles, Two-phase flow across a bank of hydrofoil micro pin fins, in: 9th AIAA/ASME Joint Thermophysics and Heat Transfer Conference, 2006, p. 3619.
[34] S. Krishnamurthy, Y. Peles, Cross flow boiling in micro-pin fin heat sinks, in: ASME 2007 International Mechanical Engineering Congress and Exposition, American Society of Mechanical Engineers, 2007, pp. 1055–1061.
[35] C. Woodcock, F. Houshmand, J. Plawsky, M. Izenson, D. Fogg, R. Hill, S. Phillips, Y. Peles, Piranha Pin-Fins (PPF): voracious boiling heat transfer by vapor venting from microchannels-system calibration and single-phase fluid dynamics, in: 4th Intersociety Conference on Thermal and Thermomechanical Phenomena in Electronic Systems (ITherm), IEEE, 2014, pp. 282–289.
[36] X. Yu, C. Woodcock, Y. Wang, J. Plawsky, Y. Peles, A study on flow boiling in microchannel with piranha pin fin, ASME 2015 International Technical Conference and Exhibition on Packaging and Integration of Electronic and Photonic Microsystems collocated, 2015, pp. V003T010A005-V003T010A005.
[37] A. Mohammadi, A. Koşar, Review on heat and fluid flow in micro pin fin heat sinks under single-phase and two-phase flow conditions, Nanoscale Microscale Thermophys. Eng. 22 (3) (2018) 153–197.
[38] C.J. Kuo, Y. Peles, Flow boiling of coolant (HFE-7000) inside structured and plain wall microchannels, J. Heat Transf. 131 (12) (2009) 121011.
[39] X. Yu, C. Woodcock, J. Plawsky, Y. Peles, An investigation of convective heat transfer in microchannel with Piranha pin pin, Int. J. Heat Mass Transf. 103 (2016) 1125–1132.
[40] Y. Lie, J. Ke, W. Chang, T. Cheng, T. Lin, Saturated flow boiling heat transfer and associated bubble characteristics of FC-72 on a heated micro-pin-finned silicon chip, Int. J. Heat Mass Transf. 50 (19–20) (2007) 3862–3876.
[41] A. Ma, J. Wei, M. Yuan, J. Fang, Enhanced flow boiling heat transfer of FC-72 on micro-pin-finned surfaces, Int. J. Heat Mass Transf. 52 (13–14) (2009) 2925–2931.
[42] M. Yuan, J. Wei, Y. Xue, J. Fang, Subcooled flow boiling heat transfer of FC-72 from silicon chips fabricated with micro-pin-fins, Int. J. Heat Mass Transf. 48 (7) (2009) 1416.
[43] D. Guo, J. Wei, Y. Zhang, Enhanced flow boiling heat transfer with jet impingement on micro-pin-finned surfaces, Appl. Therm. Eng. 31 (11–12) (2011) 2042–2051.
[44] V.P. Carey, Liquid Vapor Phase Change Phenomena: An Introduction to the Thermophysics of Vaporization and Condensation Processes in Heat Transfer Equipment, CRC Press, 2018.
[45] I. Savchenko, S. Stankus, Thermal conductivity and thermal diffusivity of tantalum in the temperature range from 293 to 1800 K, Thermophys. Aeromech. 15 (4) (2008) 679–682.